AGU PUBLICATIONS

JGR

Journal of Geophysical Research: Atmospheres

RESEARCH ARTICLE
10.1002/2015JD024435

Key Points:
- A 530 year long annually laminated sequence from Myanmar Maar Lake
- Elemental Ca and Sr time series indicate stronger ENSO-like variability after A.D. 1750
- ENSO and solar activity may be main critical driving forces of monsoon rainfall in the region

Supporting Information:
- Supporting Information S1

Correspondence to:
Q. Sun and G. Chu,
sunqing1616@yahoo.com;
chuguoqiang@mail.igcas.ac.cn

Citation:
Sun, Q., Y. Shan, K. Sein, Y. Su, Q. Zhu, L. Wang, J. Sun, Z. Gu, and G. Chu (2016), A 530 year long record of the Indian Summer Monsoon from carbonate varves in Maar Lake Twintaung, Myanmar, *J. Geophys. Res. Atmos.*, *121*, 5620–5630, doi:10.1002/2015JD024435.

Received 2 JAN 2016
Accepted 9 MAY 2016
Accepted article online 13 MAY 2016
Published online 28 MAY 2016

A 530 year long record of the Indian Summer Monsoon from carbonate varves in Maar Lake Twintaung, Myanmar

Qing Sun[1], Yabing Shan[1], Kyaing Sein[2], Youliang Su[3], Qingzen Zhu[3], Luo Wang[3], Jiming Sun[3], Zhaoyan Gu[3], and Guoqiang Chu[3]

[1]National Research Center of Geoanalysis, Beijing, China, [2]Myanmar Geosciences Society, Yangon, Myanmar, [3]Key Laboratory of Cenozoic Geology and Environment, Institute of Geology and Geophysics, Chinese Academy of Sciences, Beijing, China

Abstract We report an annually laminated sequence spanning the past 530 years from Maar Lake Twintaung, Myanmar. Calcareous varves appear as rhythmic units of light-colored carbonate and dark-colored biogenic-clastic lamina in the sediment. The light-colored carbonate layers are formed in the dry season due to strong evaporation and *Spirulina* blooms. The varved sequence provides a high-resolution geochemical archive of paleoclimatic variability in this tropical, data sparse area. A synchrotron radiation X-ray fluorescence method was used to analyze elemental data at seasonal to annual time scales. In this arid region, elemental Ca and Sr are mainly regulated by the balance of evaporation and precipitation in this closed lake basin. The elemental variations show distinct interannual and decadal variabilities. On interannual time scales, spectral analysis of the Ca and Sr time series indicates stronger El Niño–Southern Oscillation (ENSO)-like (Indian Ocean Dipole (IOD)-like) variability at periods of 2–7 years. It may suggest that ENSO and/or IOD are two dominant modes of regional rainfall variability on interannual time scales over the past 530 years. The quasiperiodicities of approximately 10 years suggest that solar activity may be a critical driving force of monsoonal rainfall in the region. A notable feature is that decreasing monsoonal rainfall since A.D. 1840 is coupled with tropical sea surface temperature variation. Considering that the monsoonal rainfall is coupled with several atmospheric processes evolving at different spatial and temporal scales, more high-resolution data are required to evaluate and verify the regional rainfall variability and its dynamic links.

1. Introduction

The Indian Summer Monsoon (ISM) is most important for people living in southern Asia where the economy is primarily dependent on rain-fed agriculture. Historically, South Asia has suffered many monsoonal disasters and terrible famines. For example, the monsoon disasters in Bengal in A.D. 1770 killed 10 million people [*Lal*, 2010]. For this reason, many efforts have been made to understand the nature and causes of monsoonal rainfall variability since the early part of the twentieth century [*Walker*, 1933]. The El Niño–Southern Oscillation (ENSO) and Indian Ocean Dipole (IOD) exert important effects on monsoons over the Indian subcontinent [*Saji et al*., 1999; *Sein et al*., 2015], although the teleconnections between regional rainfall and ENSO or the IOD are highly variable on both spatial and temporal time scales [*Kumar et al*., 2006; *Ashfaq et al*., 2009; *Izumo et al*., 2014]. On decadal time scales, instrumental data on monsoonal rainfall suggest that the Pacific Decadal Oscillation (PDO) may also affect drought/wet episodes in India and Myanmar [*Krishnan and Sugi*, 2003; *Sen Roy and Sen Roy*, 2011]. *Sen Roy and Sen Roy* [2011] found that the PDO modulates precipitation during ENSO events across Myanmar, with drought conditions during El Niño events in the warm PDO phase and the reverse conditions during La Niña events.

Instrumental records are too short to assess low-frequency variability beyond decadal time scales. Proxy-based reconstructions have therefore been widely used to describe such changes in a longer-term context. In the ISM region, high-resolution proxy climate records have mainly been derived from tree rings [*Cook et al*., 2008; *Buckley et al*., 2010; *D'Arrigo et al*., 2011; *Xu et al*., 2011, 2012; *Sano et al*., 2013; *Liu et al*., 2014; *Shi et al*., 2014], stalagmites [*Sinha et al*., 2011; *Berkelhammer et al*., 2014], ice cores from the southern Himalayan region [*Kaspari et al*., 2007], and a few lacustrine sedimentary records [*Chu et al*., 2011; *Rodysill et al*., 2012]. Considering these records, there are noticeable discrepancies in the variation of monsoonal rainfall among different localities. For example, the abundance of fossilized *Globigerina bulloides* in the

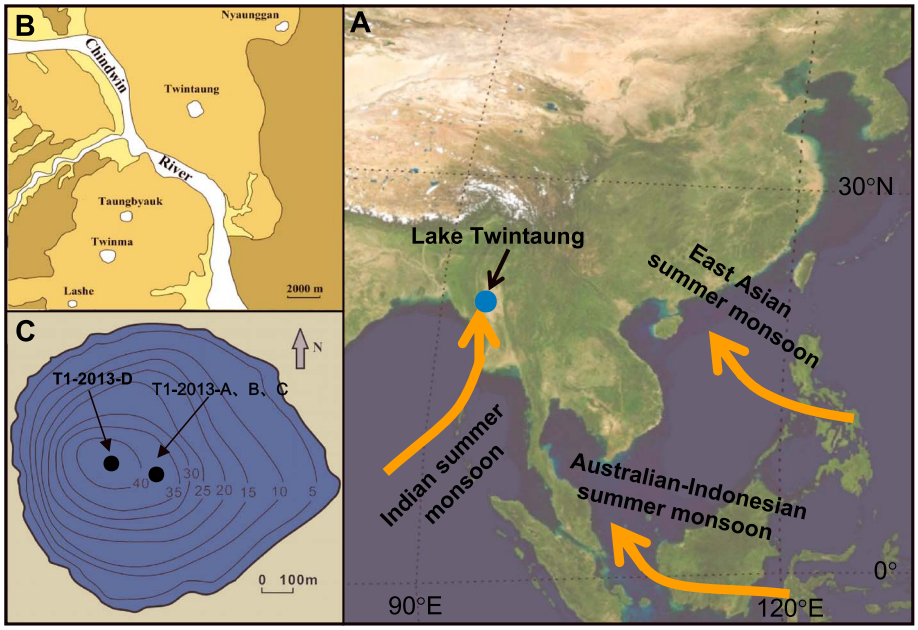

Figure 1. Location of Maar Lake Twintaung and coring site. (a) Location of Maar Lake Twintaung and moisture air masses associated with different monsoon branches to the region; (b) Geological map shows distribution of maar lakes in Myanmar. White circles: maar lake; yellow color: alluvial deposit; brown color: volcanic rocks; dark brown color: Irrawaddy formation; (c) map of Lake Twintaung showing bathymetric curve (the interval of isobathic curve is 10 m) and coring site.

Arabian Sea suggests that the ISM wind strength increased during the past four centuries [*Anderson et al.*, 2002], whereas tree ring oxygen isotope records from northern Laos and Vietnam indicate a reduction of the ISM since the late seventeenth century [*Xu et al.*, 2013]. These discrepancies may be partly due to spatial differences in monsoonal rainfall in addition to uncertainties in proxy interpretation and dating. More independent time series are therefore required to capture regional climatic variability and understand its dynamical link.

Annually laminated sediment sequences provide valuable archives for understanding high-resolution paleoclimatic changes because of their precise chronology [*Zolitschka*, 1996; *Lamoureux*, 1999; *Ojala et al.*, 2012; *Larocque-Tobler et al.*, 2015]. However, few techniques can be used to obtain high-resolution data at annual to seasonal time scales except for varve thickness. Nondestructive X-ray fluorescence (XRF) provides a powerful analytical technique to analyze elemental variations on seasonal to annual time scales [*Kalugin et al.*, 2007, 2013; *Weltje and Tjallingii*, 2008; *Francus et al.*, 2009; *Boës et al.*, 2011; *Chu et al.*, 2013].

Here we present high-resolution elemental data measured using in situ synchrotron radiation X-ray fluorescence (SRXRF) on a 530 year varved sediment section from Maar Lake Twintaung, Myanmar. The aim of this study was to capture both high-frequency and low-frequency climate variability from annually laminated sediments in this tropical region.

2. Study Site

The nearly circular Lake Twintaung (22°22′N, 95°02′E) is located in the northwestern region of the Indo-China Peninsula, Myanmar (Figure 1). The study area is in a dry zone because of a rain shadow effect. The Rakhine Yoma Mountains in the west and the Shan plateau in the east block the passage of air masses from the Indian and Pacific Oceans, respectively, creating dry conditions in the leeward basin. The climate is characterized by strong seasonality. The wet season lasts from May to November and accounts for nearly 90% of the total annual precipitation of 757 mm, whereas very little precipitation occurs during the dry season between December and May [*Htway and Matsumoto*, 2011]. The mean annual air temperature of the area is approximately 27°C. The hottest months are in March, April and May, often with maximum temperatures above 40°C.

Lake Twintaung was formed by alkali basaltic phreatomagmatic eruptions in the early Quaternary [*Sun et al.*, 2015]. The catchment area is 2.2 km^2, and the lake has a surface area of 0.8 km^2 and a maximum deep depth

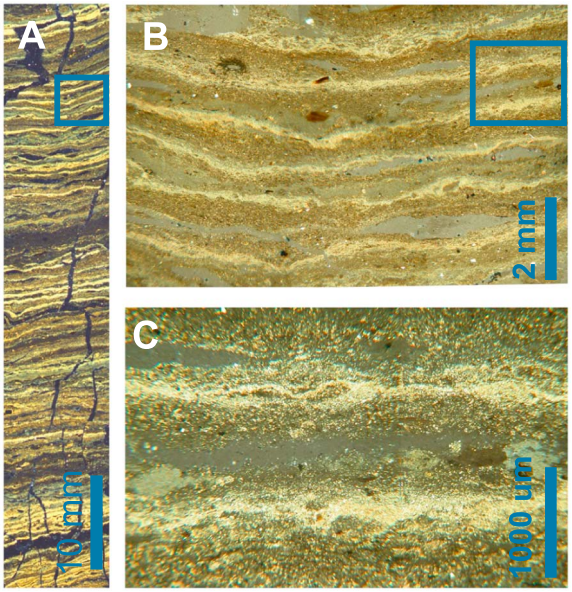

Figure 2. Photomicrographs of carbonate varves. (a) Microphotographs under a stereoscopic microscope (with polarized and transmitted light); (b) detail of laminations from a marked area in Figure 2a under a Leitz light microscope; (c) Detail of laminations from a marked area in Figure 2b.

of 50 m. The lake was stratified with a hypoxic bottom below 5 m in October 2013 and March 2014 (Figure S1 in the supporting information). The temperature and pH (in October 2013) varied from 22°C and 9.57 at the bottom to 30°C and 9.75 at the surface, respectively. The conductivity decreased from 4.77 mS/cm at the lake bottom to 4.55 mS/cm near the surface (Figure S1). *Spirulina* naturally blooms in this alkaline lake. Local people have collected *Spirulina* as a medicinal product from Lake Twintaung (Myanmar Pharmaceutical Factory) since A.D. 1987.

3. Methods

3.1. Sediment Coring

Core X2013-B1 was used in this study. The coring sites are shown in Figure 1. The corer was carefully operated and allowed to slowly penetrate the sediment due to gravity to recover a complete and undisturbed record of the uppermost sediments. In the field, the water in the upper part of the coring tube was carefully removed using a hose and paper towels. In the laboratory, the cores were dried further by inserting paper towels before the cores were split open.

3.2. Varves and Radiometric Dating

To prepare thin sections, overlapping sediment slabs 13 cm in length were cut with a 2.0 cm overlap, shock-frozen with nitrogen, vacuum-dried and impregnated with epoxy resin. Scales in centimeters were marked on the thin sections with a pencil. Laminations were identified and counted from the thin sections under a Leitz polarizing microscope and a stereoscopic microscope. The minimum varves and maximum chronology were based on the counting varves 4 times by two investigators. Based on the repeated counts by different investigators, the error of the varve chronology (the difference between the maximum and minimum values) was less than 3%. Radiometric dating (^{137}Cs, ^{210}Pb) was presented in an earlier study [*Sun et al*., 2015].

Three radiocarbon data were obtained by accelerator mass spectrometry on leaf and charcoal samples at the Poznan Radiocarbon Laboratory in this study. A chemical pretreatment (acid-alkali-acid) method was used to remove humic and fulvic acids and carbonates deposited in the organic fractions of sediments before measurement. The AMS ^{14}C ages were converted to calendar ages using the atmospheric data set from the calibration program CALIB 4.03 [*Stuiver et al*., 1998].

3.3. Synchrotron Radiation X-ray Fluorescence In Situ Analysis

The sediment blocks (60 × 10 × 5 mm) were taken from the core using aluminum trays and allowed to dry for approximately 2 days before analysis. The SRXRF measurements were performed at the hard X-ray beamline BL15U of the Shanghai Synchrotron Radiation Facility (SSRF). The sediment block was fixed on a seven-axis sample stage, which was driven by step motors. An incident beam energy of 19.98 keV was used for the determination of elements with atomic masses less than that of Mo. The beam size was 80 × 100 μm in length and width, respectively. A seven-element Si (Li) detector was used to collect the SRXRF signals from the samples with scan time of 20 s. The European Synchrotron Radiation Facility (ESRF) freely provided the Python Multichannel analyzer (PyMca) that was used to fit the measured SRXRF spectra from the sediments. The fitted peak area was normalized to the region of interest (ROI) from 110 to 250 channels. The ROI is a method used to define an elemental X-ray spectrum, generate a quantitative elemental map, and obtain the sum of all the X-ray counts from a selected region. Matrix effects were corrected using Compton scattered

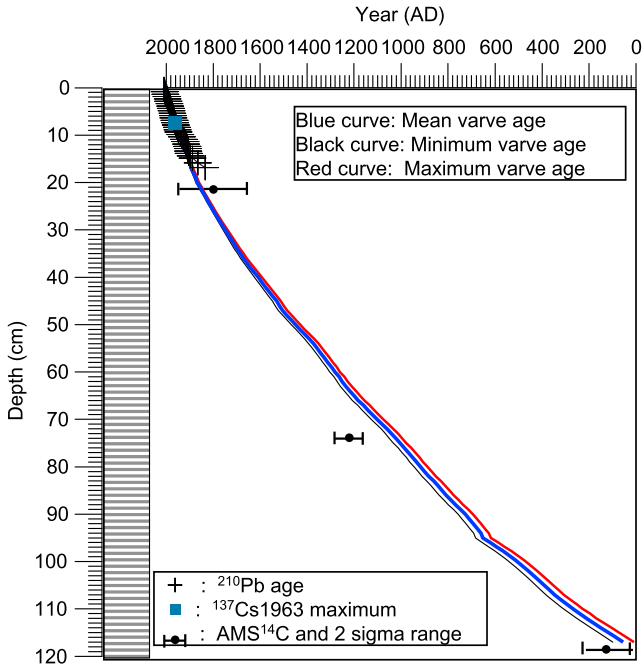

Figure 3. Varve age and radiometric dating data (^{137}Cs, ^{210}Pb, and AMS^{14}C) versus sediment core depth. The data of ^{137}Cs, and ^{210}Pb are from *Sun et al.* [2015].

radiation. Chinese national standard materials molded as sample blocks were used to control the analysis quality. Normalized elemental intensities (Br, Rb, Sr, Zr, Ti, Fe, Mn, Cu, Zn, and K) were hence obtained. After standardization, the relative standard deviations of the elemental intensities (Br, Rb, Sr, Zr, Ti, Fe, Mn, Cu, Zn, and K) were better than 15%. The ages of the SRXRF data were transferred from the varve chronology established on the thin sections.

4. Results and Discussion

4.1. Varve Formation and Varve Chronology

Initial inspection of the fresh split surface of the cores revealed millimeter-scale, light- and dark-colored laminated couplets. The light-colored layers were composed mainly of calcite crystals with thicknesses ranging from 50 μm to 400 μm, and the dark-colored layers consisted of organic and siliceous matter (Figure 2). A previous study has suggested that calcite crystals deposit due to strong evaporation and *Spirulina* blooms in the dry season, whereas clastic and organic matter are deposited during the wet season [*Sun et al.*, 2015]. In the dry season, calcite crystals form due to less precipitation and strong evaporation. In addition, algal blooms could intensify the endogenic precipitation of carbonate crystals due to photosynthetic activity. In the wet season, summer precipitation causes floods that transport more minerogenic detritus into the lake.

Calcareous varves have been found not only in lakes under temperate climatic conditions [*Livingstone and Hajdas*, 2001; *Zhou et al.*, 2007; *Bluszcz et al.*, 2009; *Ariztegui et al.*, 2010] but also in tropical lakes [*Shanahan et al.*, 2008; *Kienel et al.*, 2009; *Bird et al.*, 2011]. In humid climates, calcareous varves (carbonaceous-biogenic varve) result from seasonal biological activity that induces the precipitation of calcite crystals in the lake [*Zolitschka et al.*, 2015]. In arid regions, calcareous varves (or evaporitic varves) are related to high levels of evaporation, which increase ion concentrations in lake water [*Brauer*, 2004]. At Lake Twintaung, *Spirulina* has naturally bloomed between February and April each year (between 1987 and 2013). Local people harvest *Spirulina* as a medicinal product (Prof. Min Then, a Myanmar algae scientist and manager of the Myanmar *Spirulina* Factory, provided the information about *Spirulina* blooms). In Lake Twintaung, two processes (seasonal biological blooms and evaporation) combine in the dry season between December and May [*Sun et al.*, 2015].

An independent chronology previously derived from ^{137}Cs and ^{210}Pb shows good agreement with the counted laminations over the past 100 years in Lake Twintaung [*Sun et al.*, 2015]. Figure 3 shows the varve chronology and independent radiometric dating results (^{137}Cs, ^{210}Pb and AMS^{14}C) versus depth for Lake Twintaung. The varve chronology roughly corresponds to the radiometric dating data within the error (^{137}Cs, ^{210}Pb and AMS^{14}C) (Figure 3). An AMS^{14}C age at 74 cm is significantly younger than the varve age, which may be due to the small amount dating material (0.6 mg C) used.

4.2. Elemental Variation and Interpretation

Figure 4 shows the time series of selected major and trace elements (Sr, Ca, K, Ti, Rb, Zr, Fe, Mn, Cu, Zn, and Br) since A.D. 1480 in the sediment sequence of Lake Twintaung (Figure 4). Principal component analysis (PCA) was used to understand the relationship among different elements. This statistical technique has been

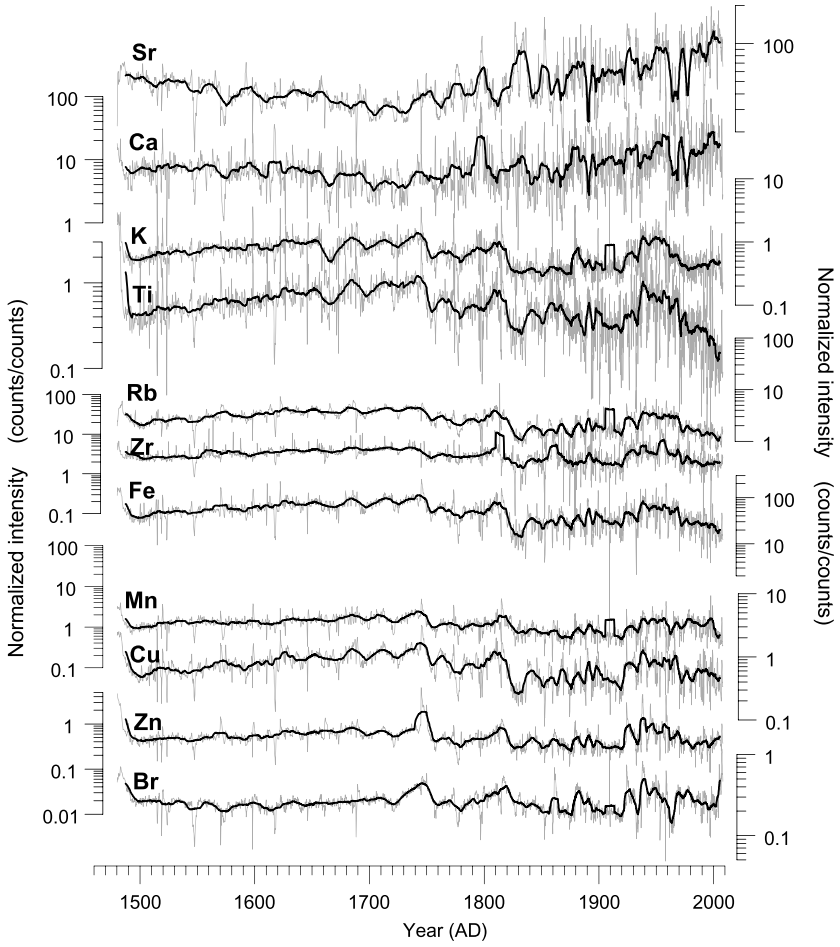

Figure 4. Time series of series of Sr, Ca, K, Ti, Rb, Zr, Fe, Mn, Cu, Zn, and Br. The elemental concentration is normalized intensity (counts/counts). Black lines are 51-point running average.

successfully used to study geochemical data sets to understand the structure of the variance of the parameters [*Chu et al.*, 2013]. Table 1 lists the PCA scores (Table 1). Based on the PCA results, the first component includes the elements K, Ti, Mn, Fe, Cu, Zn, and Rb, which primarily originate from lithogenic materials in volcanic areas and are mainly regulated by physical and chemical weathering processes [*Chu et al.*, 2013]. A broadly similar variation can be observed for K, Ti, Rb, Zr, Fe, Mn, and Cu (Figure 4).

Table 1. Rotated Matrix Component of Elements[a]

Element\Factor	Factor 1	Factor 2	Factor 3
K	0.909	0.098	0.073
Ca	0.078	0.865	0.028
Ti	0.813	−0.105	0.045
Mn	0.836	0.044	0.115
Fe	0.910	−0.250	0.129
Cu	0.861	−0.238	0.288
Zn	0.709	0.058	0.428
As	0.518	0.242	0.369
Br	0.382	0.088	0.734
Rb	0.738	−0.419	0.125
Sr	−0.312	0.796	0.247
Zr	0.031	−0.355	0.328
Pb	0.070	0.037	0.798
% of Variance	45.5	15.5	8.4

[a]Extraction method: Principal Component Analysis; Rotation method: Varimax with Kaiser Normalization.

The second component includes Ca and Sr, the variations of which are correlated with a coefficient of 0.62 (Pearson coefficient, $r = 0.62$, $p < 0.001$). Elemental Ca and Sr have been shown to be excellent paleoclimate indicators and have been widely used to reconstruct lacustrine salinity or paleotemperature data [*Mischke et al.*, 2005; *Zhang et al.*, 2009; *Kalugin et al.*, 2013]. In Lake Twintaung, the carbonates are of authigenic origin because there are

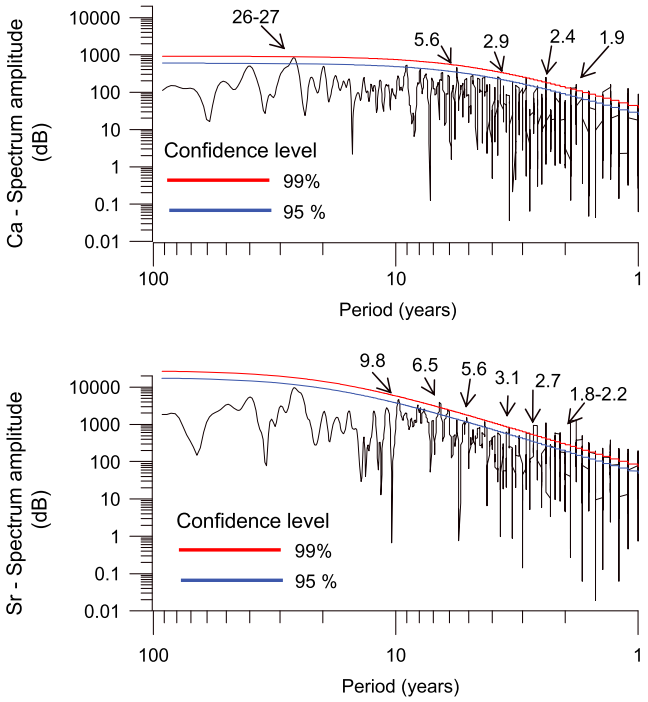

Figure 5. Spectral analysis results of the elemental (top) Ca and (bottom) Sr time series. The spectra were estimated using the program REDFIT [*Schulz and Mudelsee*, 2002] with OFAC = 4 and HIFAC = 1. The 1000 Monte Carlo simulations were used for the bias correction. The spectral window is a Welch E type. The red-noise alternative is upper 95% bound (smooth line) from a first-order autoregressive (AR1) process.

no carbonates in the watershed of this maar lake. Strontium has the proper charge and ionic radius to substitute freely for Ca^{2+} in the calcite and dolomite lattice, as well as in the lattice of other minerals such as strontianite and Kalistronite. Furthermore, strontium is a mobile element with similar geochemical behavior to calcium in natural systems. These above mentioned reasons explain why these elements are highly correlated.

Strong evaporation of lake water under arid climatic conditions can increase the salinity and pH, resulting in carbonate precipitation and carbonaceous varve formation in arid and semiarid regions [*Zhou et al*., 2007; *Shanahan et al*., 2008; *Kienel et al*., 2009; *Zolitschka et al*., 2015]. For example, carbonaceous varves have been reported in the tropical Maar Lake Hoya La Alberca, Mexico [*Kienel et al*., 2009] and in a crater, Lake Bosumtwi, Ghana [*Shanahan et al*., 2008]. Some lakes under temperate and humid climatic conditions can also be saturated with calcium carbonate due to the temperature-related increase of photosynthetic activity in the water column [*Zolitschka et al*., 2015]. As the temperature increases and spring algae blooms occur, photosynthesis consumes CO_2, which increases the pH and facilitates carbonate precipitation. Modern observations have shown that *Spirulina* naturally blooms between primarily February and April. A negative correlation was obtained between the precipitation observed at a local weather station and the variation in Ca (Pearson = 0.39, $n = 82$, $p < 0.05$) [*Sun et al*., 2015] (Figure S2 in the supporting information).

The third component includes Br and Zn, typical biogenic source minor elements. The element Br is positively correlated with Zn (Pearson coefficient, $r = 0.59$, $p < 0.001$). Bromine is essential for the growth of plants, bacteria, and plankton. In lake sediments, Br mainly originates from biogenic matter in soil and plankton in the lake [*Leonova et al*., 2011]. In Lake Kirek, the planktonogenic source of the influx of P, Br, and Zn to ferruginous sapropel appeared to be dominant (95–53%) [*Leonova et al*., 2011]. *Phedorin et al*. [2000] proposed that Br is a new proxy of the paleoproductivity of Lake Baikal. Warmer temperature and higher precipitation would increase the mobility of Br from soil in the catchment. In Lake Teletskoye, a positive correlation was observed between the Br concentration and annual temperature [*Kalugin et al*., 2007]. In our study region, the mean annual air temperature is approximately 27°C with little variation. Temperature may not be a main factor influencing biogenic production. In addition, there was no significant relation between precipitation and the Br concentration over the past 100 years.

4.3. High- and Low-Frequency Climate Variability

The spectral analysis [*Schulz and Mudelsee*, 2002] of Ca indicates several high-frequency quasiperiodicities (1.9, 2.4, 2.9, 3.8, 5.6, and 9.0 years) and a low-frequency periodicity (26–27 years) at a confidence level greater than 95% (Figure 5). In the Sr time series, quasiperiodicities (1.8–2.2, 2.4, 2.7, 3.1, 5.1, and 6.5 years) and a low-frequency periodicity (9.7–9.8 years) were also detected at a confidence level greater than 95% (Figure 5). The high-frequency variability (2 to 7 years) in the Sr and Ca time series is similar to the ENSO and IOD periodicities. Both the IOD and ENSO show high-frequency variance at biennial (~2 years) and interannual (~3 years, 5–7 years) periods [*Abram et al*., 2008].

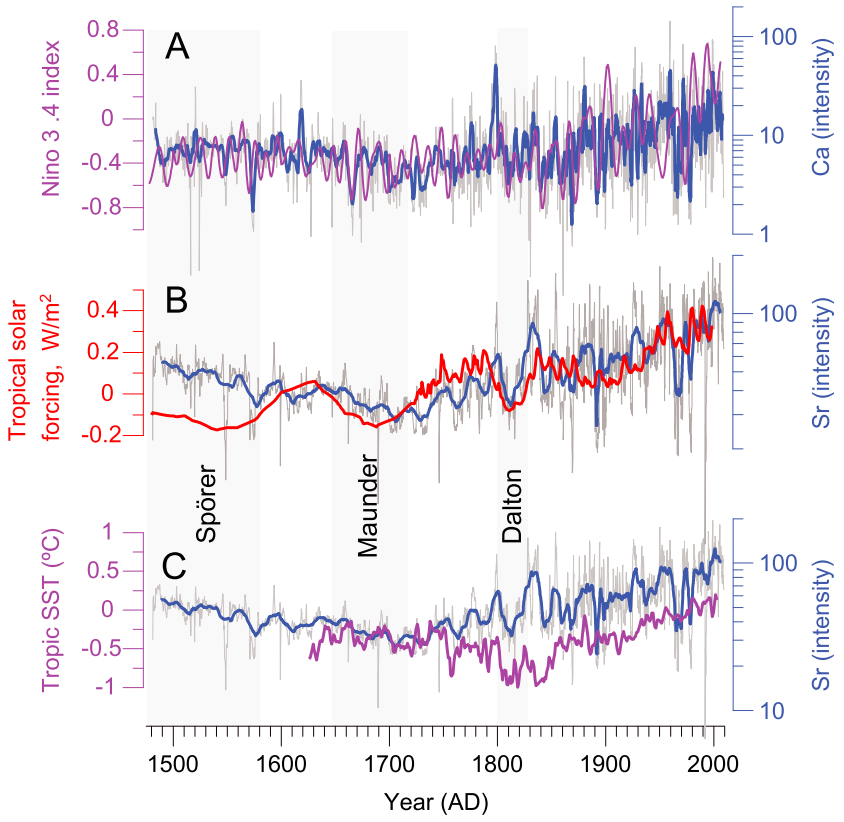

Figure 6. Comparison of the variations of elemental time series, Niño 3 index, solar radiative forcing, and tropical SST. (a) Ca time series (blue line is 15-point running average) in this study; Niño 3.4 index (purple) is from *Mann et al.* [2009]; (b) Sr time series (blue line is 61-point running average) in this study; tropical solar radiative forcing (red line is three-point running average) is from *Mann et al.* [2005]. The tropical solar radiative forcing is relative to A.D. 1000–1999 mean; (c) Sr time series (blue line is 61-point running average) in this study; the tropical SST (red line is three-point running average) is from *Tierney et al.* [2015]. The grey bars indicate the solar activity minima.

Instrumental data indicate that rainfall over Myanmar is positively correlated with the Southern Oscillation Index and negatively correlated with the IOD [*Sen Roy and Sen Roy*, 2011; *Sein et al.*, 2015]. Generally, El Niño events and negative IOD phases result in drought conditions in the region, whereas La Nina events and positive IOD phases result in flooding [*Sein et al.*, 2015]. The drought conditions associated with the warm phases of ENSO might be due to an anomalous regional Hadley circulation cell with descending motion over the Indian continent and ascending motion near the equator sustained by the ascending phase of the anomalous Walker circulation over the equatorial Indian Ocean [*Krishnamurthy and Goswami*, 2000].

ENSO-like variability has been inferred from many tree ring records [*Cook et al.*, 2008; *Buckley et al.*, 2010; *D'Arrigo et al.*, 2011; *Xu et al.*, 2013; *Liu et al.*, 2014] and lacustrine sediments [*Chu et al.*, 2011] in the ISM region. Based on a chronology of tree ring $\delta^{18}O$ in northern Laos, *Xu et al.* [2013] reconstructed local ENSO events during the last 400 years. Myanmar teak growth was below average during the late Victorian Great Drought, which was associated with a major ENSO warm event (1876 to 1878) [*Cook et al.*, 2013]. A tree ring index in southwestern China [*Shi et al.*, 2014] recorded two historic major drought events that occurred during the eighteenth (A.D. 1790–1796) and the nineteenth (A.D. 1876–1877) centuries and are believed to have been a response to a period of severe El Niño events.

Figure 6a compares the Ca time series in this study with the Niño 3.4 series [*Mann et al.*, 2009]. A generally similar pattern can be observed in the elemental time series and ENSO index during the past 530 years. Some of the higher Ca and Sr values coincided with stronger El Niño years. For example, stronger El Niño events that occurred in 1997–1998, 1982–1983, 1957–1958, 1925–1926, and historically severe drought years occurred in A.D. 1790–1796 and A.D. 1876–1877 (Figures S2 and 6a). However, not all El Niño events could be

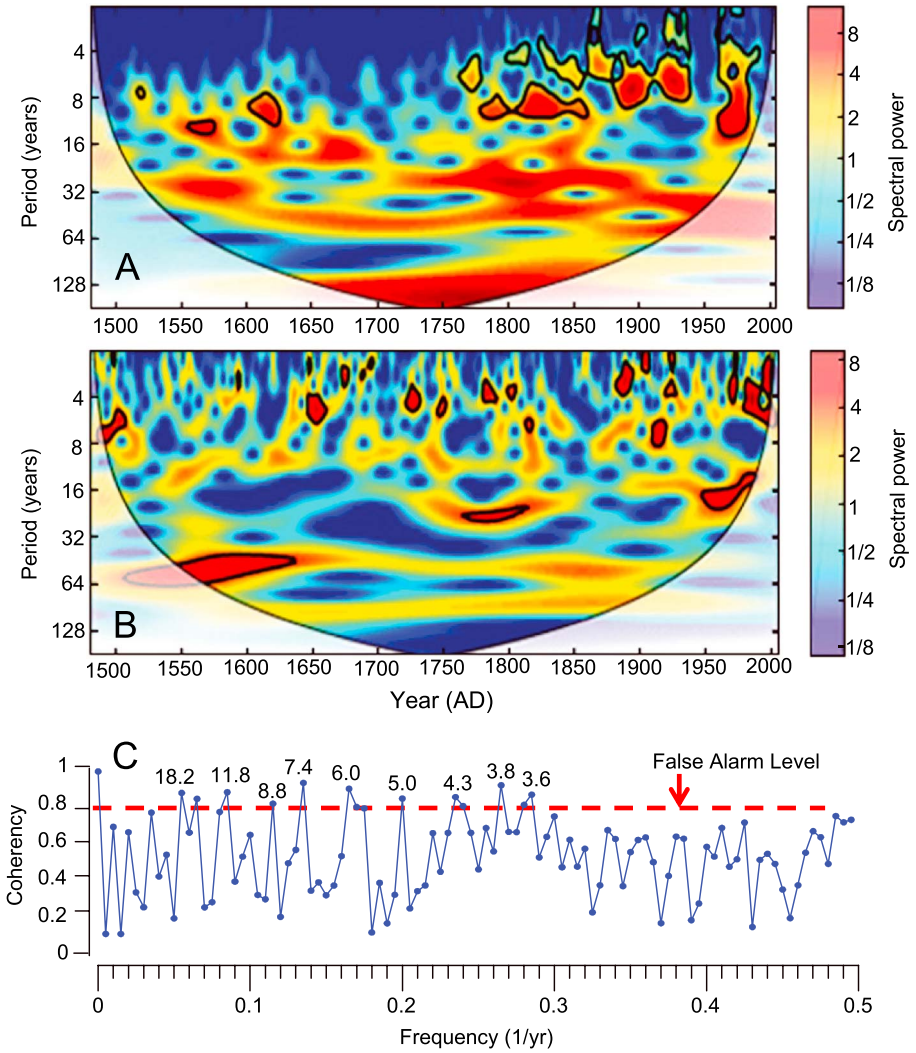

Figure 7. Continuous wavelet power spectrum and coherency of the standardized Ca and Niño 3.4 time series. (a) Continuous wavelet transform of the standardized Ca time series. The black line shows the 95% confidence level; (b) Continuous wavelet transform of the standardized Niño 3.4 series [*Mann et al.*, 2009]. Niño 3.4 index is from *Mann et al.* [2009]. The black line shows the 95% confidence level; (c) Coherency spectrum (solid line) from cross-spectral analysis of both time series. Significant peaks above the 80% false alarm level (dashed horizontal line).

detected in the Ca and Sr time series. There are uncertainties in the varve chronology and the process by which we convert the varve chronology to an elemental time scale.

In order to calculate coherence between the Ca time series and Niño 3.4 series [*Mann et al.*, 2009], we used the Arand software package [*Howell*, 2001] to conduct cross-spectral analyses. Figure 7 shows the continuous wavelet transform (CWT) of both standardized time series from 1480 A.D. to 2006 A.D. (Figures 7a and 7b). Both series have high power in the 2–7 year band. The 2–7 year band in the Ca time series is significant between A.D. 1750 and A.D. 2006 but is lower before A.D. 1750. Cross-spectral analysis of the Ca time series and Niño 3.4 series have matching periodicities at 18.2,, 11.8, 8.8, 7.4*r*, 6.0, 5.0, 4.3, 3.8, and 3.6 years above 80% confidence, respectively (Figure 7c). Although the coherence between the two reconstructed records confirms the close relationship between regional rainfall and ENSO, similarity in two time series is quite low. It could be due to the teleconnection between ENSO and Indian monsoonal rainfall that is nonstationary through time [*Kumar et al.*, 2006; *Berkelhammer et al.*, 2014]. In addition to ENSO, other factors (such as solar activity, the PDO and the IOD) can also affect the hydroclimatic variability [*Kumar et al.*, 2006; *Izumo et al.*, 2014; *Berkelhammer et al.*, 2014].

The spectrum also exhibits a broad, lower frequency energy spectrum at decadal scales (9.8, 26–27 years) (Figure 5). The 11 year cycle of solar forcing leads to changes in atmospheric or oceanic circulation. *Meehl et al.* [2009] proposed that cloud feedback at low latitudes can amplify the Pacific climate system in response to a small 11 year solar cycle forcing. Relatively low values of Sr and Ca correspond well to two solar activity minima in the Dalton Minimum (A.D. 1798 to 1823) and the Maunder Minimum (A.D. 1645 to 1715), but they are not pronounced in the Spörer Minimum (A.D. 1460–1600) (Figure 6b).

A quasiperiodicity of approximately 11 years has been detected in a few high-resolution proxy records from tropical regions. For example, spectral analysis of the Ca^{2+} time series from an ice core from Mount Everest ice core revealed periodicities at 2–4 and 9.0 years [*Kaspari et al.*, 2007]. A high-resolution stalagmite $\delta^{18}O$ record in Oman indicated significant cycles of approximately 12 years [*Burns et al.*, 2002]. *Charles et al.* [1997] presented a 150 year long coral $\delta^{18}O$ record from Mahe Island and documented decadal periodicities (11.8 to 12.3 years).

In addition to the ENSO impact and solar forcing, other internal dynamics (e.g., ocean circulation) should also play crucial roles in regional climate changes. The PDO has been recognized as a major driver of decadal to multidecadal climatic variability for the Pacific region [*MacDonald and Case*, 2005]. In the ISM region, proxy records from tree rings have detected strong PDO–like variability [*Cook et al.*, 2013; *Sano et al.*, 2013; *Liu et al.*, 2014]. The 27 year quasiperiodicity in this study is similar to tree ring reconstructions in Pakistan [*Cook et al.*, 2013] and Myanmar [*D'Arrigo and Ummenhofer*, 2015]. However, the underlying mechanism is not clear.

Sea surface temperature (SST) is a primary driver of oceanic–atmospheric anomalies and is applied in most monsoon forecasting modes. Figure 6c shows a comparative diagram of the tropical SST from high-resolution coral archives [*Tierney et al.*, 2015] and the elemental Sr record. The elemental variations exhibit a similar pattern as that of the tropical SST (Figure 6c). The increasing trend of elemental Ca and Sr suggests a decreasing monsoonal rainfall since A.D. 1840 (Figure 6c). A similar decreasing pattern can be observed across different proxy records and different localities from the southeastern Tibetan Plateau, such as the varved sediments from Lake Xingluhai [*Chu et al.*, 2011], and in tree ring $\delta^{18}O$ records from the ISM region [*Xu et al.*, 2012; *Sano et al.*, 2012; *Xu et al.*, 2013]. The link may be the same air mass that flows over the Bay of Bengal and passes through our study region, penetrating into the southeastern Tibet Plateau. A model-based study suggested that the summertime weakening in the SST gradient weakens the monsoonal circulation, resulting in less monsoonal rainfall over India and excess rainfall over sub-Saharan Africa [*Chung and Ramanathan*, 2006]. Recently, *Ali et al*. [2013] studied the statistical relationship between cyclone intensity and SST in the tropical Indian Ocean and demonstrated that more than 50% of the north Indian Ocean tropical cyclone intensities are negatively correlated with SST [*Ali et al.*, 2013].

Considering that ISM rainfall is coupled with several atmospheric processes evolving at different spatial and temporal scales, more high-resolution data are required to evaluate and verify the regional rainfall variability and its dynamic links.

5. Conclusions

We report a high-resolution proxy record spanning the past 530 years from an annually laminated sequence in Maar Lake Twintaung, Myanmar. The varves consisted of light- and brown-colored laminae couplets. The light-colored layers were composed mainly of calcite crystals that had formed in the dry season due to strong evaporation and *Spirulina* blooms in the lake. In this semiarid region, the elemental Ca and Sr contained in this closed lake are mainly regulated by the balance between evaporation and precipitation.

The SRXRF method was used to analyze the elemental data on seasonal to annual time scales. The elemental variations exhibit distinct high-frequency and low-frequency climate variability. On the interannual time scale, the spectral analysis of the Ca and Sr time series indicates stronger ENSO-like variability at 2–7 years.. On decadal time scales, the quasiperiodicities of approximately 10 years suggest that solar activity may be a critical driving force of monsoonal rainfall in the region.

The increasing trend of elemental Ca and Sr suggests decreasing monsoonal rainfall since A.D. 1840. This trend is similar to the tropical SST variation since A.D. 1840. Considering that ISM rainfall is coupled with several atmospheric processes evolving at different spatial and temporal scales, more high-resolution data are required to evaluate and verify the regional rainfall variability and its dynamic links.

Acknowledgments

This research was jointly supported by the National Natural Science Foundation of China under grants 41371219 and 41272198 and the Strategic Priority Research Program of the Chinese Academy of Sciences (XDB03020000). We thank Min Then, Win Swe, Zaw Win, and Than Zaw for help in field sampling. Niño 3.4 data in Figure 6a are derived from www.sciencemag.org/cgi/content/full/326/5957/1256/DC1 [*Mann et al.*, 2009]. Tropical solar radiative forcing data in Figure 6b are available through the NOAA Climate Forcing website (http://www.ncdc.noaa.gov/data-access/paleoclimatology-data/datasets/climate-forcing) [*Mann et al.*, 2005]. The tropical SST data in Figure 6c are from ftp://ftp.ncdc.noaa.gov/pub/data/paleo/pages2k/tierney2015 [*Tierney et al.*, 2015]. The elemental data in this paper are available upon request to the corresponding author at chugoqiang@mail.iggcas.ac.cn. We would like to thank three anonymous reviewers and Deke Xu for constructive comments and correcting English. We also acknowledge the members of the SSRF Synchrotron Radiation Facility.

References

Abram, N. J., M. K. Gagan, J. E. Cole, W. S. Hantoro, and M. Mudelsee (2008), Recent intensification of tropical climate variability in the Indian Ocean, *Nat. Geosci.*, *1*, 849–853.

Ali, M. M., D. Swain, T. Kashyap, J. P. McCreary, and P. V. Nagamani (2013), Relationship between cyclone intensities and sea surface temperature in the tropical Indian Ocean, *IEEE Geosci. Remote Sens. Lett.*, *10*, 841–844.

Anderson, D. M., J. T. Overpeck, and A. K. Gupta (2002), Increase in the Asian Southwest monsoon during the past four centuries, *Science*, *297*, 596–599.

Ariztegui, D., F. S. Anselmetti, J. M. Robbiani, S. M. Bernasconi, E. Brati, A. Gilli, and M. Lehmann (2010), Natural and human-induced environmental change in Southern Albania for the last 300 years—Constraints from the Lake Butrint sedimentary record, *Global Planet. Change*, *71*, 183–192.

Ashfaq, M., Y. Shi, W. Tung, R. J. Trapp, X. Gao, J. S. Pal, and N. S. Diffenbaugh (2009), Suppression of south Asian summer monsoon precipitation in the 21st century, *Geophys. Res. Lett.*, *36*, L01704, doi:10.1029/2008GL036500.

Berkelhammer, M., A. Sinha, M. Mudelsee, H. Cheng, K. Yoshimura, and J. Biswas (2014), On the low-frequency component of the ENSO–Indian monsoon relationship: A paired proxy perspective, *Clim. Past*, *10*, 733–744.

Bird, B. W., M. B. Abbott, M. Vuille, D. T. Rodbell, N. D. Stansell, and M. F. Rosenmeier (2011), A 2,300-year-long annually resolved record of the South American summer monsoon from the Peruvian Andes, *Proc. Natl. Acad. Sci. U.S.A.*, *108*, 8583–8588.

Bluszcz, P., A. Lücke, C. Ohlendorf, and B. Zolitschka (2009), Seasonal dynamics of stable isotopes and element ratios in authigenic calcites during their precipitation and dissolution, Sacrower See (northeastern Germany), *J. Limnol.*, *68*, 257–273.

Boës, N., J. Rydberg, A. Martinez-Cortizas, R. Bindler, and I. Renberg (2011), Evaluation of conservative lithogenic elements (Ti, Zr, Al, and Rb) to study anthropogenic element enrichments in lake sediments, *J. Paleolimnol.*, *46*, 75–87.

Brauer, A. (2004), Annually laminated lake sediments and their palaeoclimatic relevance, in *The Climate in Historical Times, Towards a Synthesis of Holocene Proxy Data and Climate Models*, edited by H. Fischer et al., pp. 111–129, Springer, Berlin.

Buckley, B. M., K. J. Anchukaitis, D. Penny, R. Fletcher, E. R. Cook, M. Sano, C. N. Le, A. Wichienkeeo, T. M. Ton, and M. H. Truong (2010), Climate as a contributing factor in the demise of Angkor, Cambodia, *Proc. Natl. Acad. Sci. U.S.A.*, *107*, 6748–6752.

Burns, S. J., D. Fleitmann, M. Mudelsee, U. Neff, A. Matter, and A. Mangini (2002), A 780-year annually resolved record of Indian Ocean monsoon precipitation from a speleothem from south Oman, *J. Geophys. Res.*, *107*(D20), 4434, doi:10.1029/2001JD001281.

Charles, C. D., D. E. Hunter, and R. G. Fairbanks (1997), Interaction between the ENSO and the Asian monsoon in a coral record of tropical climate, *Science*, *277*, 925–928.

Chu, G., et al. (2011), Evidence for decreasing south Asian summer monsoon in the past 160 years from varved sediment in Lake Xinluhai, Tibetan Plateau, *J. Geophys. Res.*, *116*, D02116, doi:10.1029/2010JD014454.

Chu, G., Q. Sun, S. Li, Y. Lin, W. Wang, M. Xie, W. Shang, A. Li, and K. Yang (2013), Minor element variations during the past 1300 years in the varved sediments of Lake Xiaolongwan, northeastern China, *GFF*, *135*, 229–339.

Chung, C. E., and V. Ramanathan (2006), Weakening of North Indian SST gradients and the Monsoon Rainfall in India and the Sahel, *J. Clim.*, *19*, 2036–2045.

Cook, E. R., R. D. D'Arrigo, and K. J. Anchukaitis (2008), ENSO reconstructions from long tree-ring chronologies: Unifying the differences?, paper presented at a Special Workshop on "Reconciling ENSO Chronologies for the Past 500 Years", Moorea, French Polynesia, April 2–3.

Cook, E. R., J. Palmer, M. Ahmed, C. Woodhouse, P. Fenwick, M. Zafar, M. Wahab, and N. Khan (2013), Five centuries of upper Indus River flow from tree rings, *J. Hydrol.*, *486*, 365–375.

D'Arrigo, R., and C. C. Ummenhofer (2015), The climate of Myanmar: Evidence for effects of the Pacific Decadal Oscillation, *Int. J. Climatol.*, *35*, 634–640.

D'Arrigo, R., J. Palmer, C. C. Ummenhofer, N. N. Kyaw, and P. Krusic (2011), Three centuries of Myanmar monsoon climate variability inferred from teak tree rings, *Geophys. Res. Lett.*, *38*, L24705, doi:10.1029/2011GL049927.

Francus, P., H. Lamb, T. Nakagawa, M. Marshall, E. Brown, and Suigetsu 2006 Project Members (2009), The potential of high-resolution X-ray fluorescence core scanning: Applications in palaeolimnology, *PAGES News*, *17*, 93–95.

Howell, P. (2001), *ARAND Time Series and Spectral Analysis Package for the Macintosh, Brown University, IGBP PAGES/World Data Center Paleoclimatol. Data Contrib. Ser.*, vol. 44, NOAA/NGDC Paleoclimatol. Program, Boulder, Colo.

Htway, O., and J. Matsumoto (2011), Climatological onset dates of summer monsoon over Myanmar, *Int. J. Climatol.*, *31*, 382–393.

Izumo, T., M. Lengaigne, J. Vialard, J. J. Lup, T. Yamagata, and G. Madec (2014), Influence of Indian Ocean Dipole and Pacific recharge on following year's El Niño: Interdecadal robustness, *Clim. Dyn.*, *42*, 291–310.

Kalugin, I., D. Daryin, L. Smolyaninova, A. Andreev, B. Diekmann, and O. Khlystov (2007), 800-yr-long records of annual air temperature and precipitation over southern Siberia inferred from Teletskoye Lake sediments, *Quat. Res.*, *67*, 400–410.

Kalugin, I., A. Darin, D. Rogozin, and G. Tretyakov (2013), Seasonal and centennial cycles of carbonate mineralisation during the past 2500 years from varved sediment in Lake Shira, South Siberia, *Quat. Int.*, *290-291*, 245–252.

Kaspari, S., et al. (2007), Reduction in northward incursions of the South Asian monsoon since 1400 AD inferred from a Mt. Everest ice core, *Geophys. Res. Lett.*, *34*, L16701, doi:10.1029/2007GL030440.

Kienel, U., et al. (2009), First lacustrine varve chronologies from Mexico: Impact of droughts, ENSO and human activity since AD 1840 as recorded in maar sediments from Valle de Santiago, *J. Paleolimnol.*, *42*, 587–609.

Krishnamurthy, V., and B. N. Goswami (2000), Indian Monsoon–ENSO relationship on interdecadal times, *J. Clim.*, *13*, 579–595.

Krishnan, R., and M. Sugi (2003), Pacific Decadal Oscillation and variability of the Indian summer monsoon rainfall, *Clim. Dyn.*, *21*, 233–242.

Kumar, K. K., B. Rajagopalan, M. Hoerling, G. Bates, and M. Cane (2006), Unraveling the mystery of Indian monsoon failure during El Niño, *Science*, *314*, 115–119.

Lal, R. (2010), Climate of south Asia and the human wellbeing, in *Climate Change and Food Security in South Asia*, edited by R. Lal et al., pp. 4–11, Springer, Berlin.

Lamoureux, S. F. (1999), Spatial and interannual variations in sedimentation patterns recorded in nonglacial varved sediments from the Canadian High Arctic, *J. Paleolimnol.*, *21*, 73–84.

Larocque-Tobler, I., J. Filipiak, W. Tylmann, A. Bonk, and M. Grosjean (2015), Comparison between chironomid-inferred mean-August temperature from varved Lake Żabińskie (Poland) and instrumental data since 1896 AD, *Quat. Sci. Rev.*, *111*, 35–50.

Leonova, G. A., V. A. Bobrov, E. V. Lazareva, A. A. Bogush, and S. K. Krivonogov (2011), Biogenic contribution of minor elements to organic matter of recent lacustrine sapropels (Lake Kirek as example), *Lithol. Miner. Resour.*, *46*, 99–114.

Liu, X., G. Xu, J. Grießinger, W. An, W. Wang, X. Zeng, G. Wu, and D. Qin (2014), A shift in cloud cover over the southeastern Tibetan Plateau since 1600: Evidence from regional tree-ring $\delta^{18}O$ and its linkages to tropical oceans, *Quat. Sci. Rev.*, *88*, 55–68.

Livingstone, D. M., and I. Hajdas (2001), Climatically relevant periodicities in the thickness of biogenic carbonate varves in Soppensee, Switzerland (9740-6870 calendar yr BP), *J. Paleolimnol.*, *25*, 17–24.
MacDonald, G. M., and R. A. Case (2005), Variations in the Pacific Decadal Oscillation over the past millennium, *Geophys. Res. Lett.*, *32*, L08703, doi:10.1029/2005GL022478.
Mann, M. E., M. A. Cane, S. E. Zebiak, and A. Clement (2005), Volcanic and solar forcing of the tropical Pacific over the past 1000 years, *J. Clim.*, *18*, 417–456.
Mann, M. E., Z. Zhang, S. Rutherford, R. S. Bradley, M. K. Hughes, D. Shindell, C. Ammann, G. Faluvegi, and F. Ni (2009), Global signatures and dynamical origins of the Little Ice Age and Medieval climate anomaly, *Science*, *326*, 1256–1260.
Meehl, G. A., J. M. Arblaster, K. Matthes, F. Sassi, and H. van Loon (2009), Amplifying the Pacific climate system response to a small 11-year solar cycle forcing, *Science*, *325*, 1114–1118.
Mischke, S., D. Demske, B. Wünnemann, and M. E. Schudack (2005), Groundwater discharge to a Gobi desert lake during mid and late Holocene dry periods, *Palaeogeogr. Palaeoclimatol. Palaeoecol.*, *225*, 157–172.
Ojala, A. E. K., P. Francus, B. Zolitschka, M. Besonen, and S. F. Lamoureux (2012), Characteristics of sedimentary varve chronologies—A review, *Quat. Sci. Rev.*, *43*, 45–60.
Phedorin, M. A., E. L. Goldberg, M. A. Grachev, O. L. Levina, O. M. Khlystov, and I. P. Dolbnya (2000), The comparison of biogenic silica, Br and Nd distributions in the sediments of Lake Baikal as proxies of changing paleoclimates of the last 480 kyr, *Nucl. Instrum. Methods Phys. Res., Sect. A*, *448*, 400–406.
Rodysill, J. R., J. M. Russell, S. Bijaksana, E. T. Brown, L. O. Safiuddin, and H. Eggermont (2012), A paleolimnological record of rainfall and drought from East Java, Indonesia during the last 1,400 years, *J. Paleolimnol.*, *47*, 125–139.
Saji, N. H., B. N. Goswami, P. N. Vinayachandran, and T. Yamagata (1999), A dipole mode in the tropical Indian Ocean, *Nature*, *401*, 360–363.
Sano, M., R. Ramesh, M. Sheshshayee, and R. Sukumar (2012), Increasing aridity over the past 223 years in the Nepal Himalaya inferred from a tree-ring δ18O chronology, *Holocene*, *22*, 809–817.
Sano, M., P. Tshering, J. Komori, K. Fujita, C. Xu, and T. Nakatsuka (2013), May–September precipitation in the Bhutan Himalaya since 1743 as reconstructed from tree ring cellulose δ^{18}O, *J. Geophys. Res. Atmos.*, *118*, 8399–8410, doi:10.1002/jgrd.50664.
Schulz, M., and M. Mudelsee (2002), REDFIT: Estimating red-noise spectra directly from unevenly spaced paleoclimatic time series, *Comput. Geosci.*, *28*, 421–426.
Sein, Z. M. M., B. A. Ogwang, V. Ongoma, F. K. Ogou, and K. Batebana (2015), Inter-annual variability of summer monsoon rainfall over Myanmar in relation to IOD and ENSO, *J. Environ. Agric. Sci.*, *4*, 28–36.
Sen Roy, S., and N. Sen Roy (2011), Influence of Pacific Decadal Oscillation and El Niño-Southern Oscillation on the summer monsoon precipitation in Myanmar, *Int. J. Climatol.*, *31*, 14–21.
Shanahan, T. M., J. T. Overpeck, J. W. Beck, C. W. Wheeler, J. A. Peck, J. W. King, and C. A. Scholz (2008), The formation of biogeochemical laminations in Lake Bosumtwi, Ghana, and their usefulness as indicators of past environmental changes, *J. Paleolimnol.*, *40*, 339–355.
Shi, F., J. Li, and R. J. S. Wilson (2014), A tree-ring reconstruction of the South Asian summer monsoon index over the past millennium, *Sci. Rep.*, *4*, 6739, doi:10.1038/srep06739.
Sinha, A., M. Berkelhammer, L. Stott, M. Mudelsee, H. Cheng, and J. Biswas (2011), The leading mode of Indian Summer Monsoon precipitation variability during the last millennium, *Geophys. Res. Lett.*, *38*, L15703, doi:10.1029/2011GL047713.
Stuiver, M., P. J. Reimer, E. Bard, J. W. Beck, G. S. Burr, K. A. Hughen, B. Kromer, G. McCormac, J. van der Plicht, and M. Spurk (1998), INTCAL98 radiocarbon age calibration, 24,000–0 cal BP, *Radiocarbon*, *40*, 1041–1083.
Sun, Q., Y. B. Shan, K. Sein, Y. Su, Q. Zhu, L. Wang, J. Sun, Z. Gu, and G. Chu (2015), Carbonate varves and minor element variations during the past 100 years in Maar Lake Twintaung, Myanmar [in Chinese], *Chin. Sci. Bull.*, *60*, 1038–1047.
Tierney, J. E., N. J. Abram, K. J. Anchukaitis, M. N. Evans, C. Giry, K. H. Kilbourne, C. P. Saenger, H. C. Wu, and J. Zinke (2015), Tropical sea surface temperatures for the past four centuries reconstructed from coral archives, *Paleoceanography*, *30*, 226–252, doi:10.1002/2014PA002717.
Walker, G. (1933), Seasonal weather and its prediction, *Nature*, *132*, 805–808.
Weltje, G. J., and R. Tjallingii (2008), Calibration of XRF core scanners for quantitative geochemical logging of sediment cores: Theory and application, *Earth Planet. Sci. Lett.*, *274*, 423–438.
Xu, C., M. Sano, and T. Nakatsuka (2011), Tree-ring cellulose δ^{18}O of Fokienia hodginsii in Northern Laos: A promising proxy to reconstruct ENSO?, *J. Geophys. Res.*, *116*, D24109, doi:10.1029/2011JD016694.
Xu, C., M. Sano, and T. Nakatsuka (2013), A 400-year record of hydroclimate variability and local ENSO history in northern Southeast Asia inferred from tree-ring δ^{18}O, *Palaeogeogr. Palaeoclimatol. Palaeoecol.*, *386*, 588–598.
Xu, H., Y. Hong, and B. Hong (2012), Decreasing Asian summer monsoon intensity after 1860 AD in the global warming epoch, *Clim. Dyn.*, *39*, 2079–2088.
Zhang, J., J. A. Holmes, F. Chen, M. Qiang, A. Zhou, and S. Chen (2009), An 850-year ostracod-shell trace-element record from Sugan Lake, northern Tibetan Plateau, China: Implications for interpreting the shell chemistry in high-Mg/Ca waters, *Quat. Int.*, *19*, 119–133.
Zhou, A., F. Chen, M. Qiang, M. Yang, and J. Zhang (2007), The discovery of annually laminated sediments (varves) from shallow Sugan Lake in inland Arid China and their paleoclimatic significance, *Sci. China*, *50*, 1218–1224.
Zolitschka, B. (1996), High resolution lacustrine sediments and their potential for paleoclimatic reconstruction, in *Climatic Variations and Forcing Mechanisms of the Last 2000 Years*, edited by P. D. Jones, R. S. Bradley, and J. Jouzel, pp. 453–478, Springer, Berlin.
Zolitschka, B., P. Francus, A. E. J. Ojala, and A. Schimmelmann (2015), Varves in lake sediments—A review, *Quat. Sci. Rev.*, *117*, 1–41.